Chapter 4: Targeting Platinum to DNA Mismatches via Conjugation to a Metalloinsertor Containing a Rh—O Bond

4.1 Introduction:

Platinum anticancer agents comprise an essential component in the current repertoire of chemotherapeutics. *Cis*-platinum (II) complexes such as cisplatin (**Figure 4.1**) and its derivatives have been extremely successful in the treatment of a variety of cancers, but are also associated with a litany of severe side effects and resistance.[1-5] These side effects arise primarily as a result of the mechanism by which *cis*-platinum complexes function biologically: slow displacement of labile leaving group ligands, such as chlorides or carboxylate groups, activates the platinum center for the formation of cytotoxic, covalent adducts with DNA.[1,6] Although these complexes preferentially bind the nucleophilic *N*7 position of consecutive guanine residues to form what are known as 1,2-intrastrand crosslinks, the nature of *cis*-platinum binding is inherently nonspecific and can target the DNA of non-cancerous cells as well as malignant ones.[2] Additionally, although DNA is widely considered to be the primary therapeutic target of cisplatin, platinum (II) complexes possess the ability to react with a number of biological ligands once inside the cell, including proteins. A major source of cisplatin resistance, for example, is the chelation and subsequent inactivation by sulfur-containing molecules, such as glutathione.[7] Indeed, it is reported that only 1% of intracellular cisplatin reaches the genome.[8] The ability to tune platinum therapeutics to target specific biomarkers of cancer would be invaluable in the development of next-generation platinum drugs.

Our laboratory has focused largely on the development of octahedral rhodium (III) complexes for the targeted therapy of cisplatin-resistant cancers. These complexes

selectively bind thermodynamically destabilized sites, such as base pair mismatches, in DNA.[9] Mismatches, which arise naturally as a consequence of DNA replication, lead to cancerous mutations if left uncorrected by the complex of proteins known as the mismatch repair (MMR) machinery.[10,11] As a result, deficiencies in the MMR pathway result in a buildup of these single base lesions in the genome, leading to several types of cancer. These malignancies are largely resistant to cisplatin and other classical chemotherapeutics, as MMR is also one of the DNA repair pathways that recognizes and processes cisplatin-DNA lesions.[12]

Our rhodium complexes recognize DNA mismatches not through the formation of covalent adducts, as with *cis*-platinum therapeutics, but rather through a non-covalent binding mode that involves the insertion of a sterically expansive aromatic ligand, such as 5,6-chrysenequinone diimine (chrysi) (**Figure 4.1**) into the base stack of the duplex. This binding occurs from the minor groove at the site of the mismatch, extruding the destabilized, mismatched nucleobases from the helix out into the major groove.[13-18] This binding mode, termed metalloinsertion, targets 80% of all mismatches with over 1000-fold specificity, in all sequence contexts.[13] More recently, we have demonstrated that these metalloinsertor complexes also target mismatched DNA in genomic DNA: metalloinsertors exhibit cytotoxicity preferentially in MMR-deficient colorectal cancer cells compared to isogenically matched MMR-proficient cells, and this selectivity is contingent on the localization of these complexes to the nucleus.[19-23]

Rhodium metalloinsertors are a robust class of complexes that offer a promising alternative for targeting MMR-deficient cancers and circumventing resistance. New generations of metalloinsertors have exhibited increased potency surpassing that of

cisplatin, while still maintaining selective targeting to MMR-deficiency.[22,24] While these compounds are currently being explored as chemotherapeutic agents, they also hold promise as potential adjuvants that could confer their unique selectivity onto other therapeutic cargo. Recent efforts have focused on the development of bimetallic Rh-Pt complexes that bifunctionally target DNA through both metalloinsertion at mismatched sites as well as through the formation of covalent platinum crosslinks. Previous iterations of metalloinsertor-platinum complexes have included the conjugation of a platinum center to the rhodium complex through its inert amine ligand[25] as well as the temporary attachment of the two metal centers via the labile platinum leaving group ligand.[26]

In the case of the first generation conjugate, in which a cisplatin analogue was tethered to a rhodium metalloinsertor via an alkane-modified non-leaving group (ammine) ligand, metalloinsertion at a mismatch successfully directed platinum binding preferentially toward mismatched DNA over a well-matched duplex. However, this preferential binding was highly dependent on the presence and location of a d(GpG) site (the preferred binding site of cisplatin); if there was no d(GpG) site, or if it was inaccessible to the platinum center due to limitations in the length and flexibility of the alkyl tether, then platination levels were reduced and the complex exhibited no selectivity. Preferential platination of mismatched DNA was only achieved when the d(GpG) site was located where the tether most favored interactions between the platinum center and the DNA.[25] Unsurprisingly, this limitation reduces the applications of the conjugate in a biological system; indeed, when characterized in the isogenic HCT116N (MMR-proficient) and HCT116O (MMR-deficient) human colorectal cancer cell lines,

the conjugate displayed no selective antiproliferative activity in the MMR-deficient line and in fact exhibited a slight preference for the MMR-proficient cell line.[27]

To overcome the structural limitations of the first-generation Rh-Pt conjugate, a second-generation metalloinsertor-platinum conjugate was developed wherein the platinum (II) moiety was tethered to the rhodium metalloinsertor via its leaving group ligand. Here, platination of DNA (or other biological ligands) would not occur until the platinum subunit had dissociated from the rhodium center, thereby circumventing the limitations incurred by the alkyl linker. As a result, a d(GpG) site could become platinated irrespective of its distance from a base pair mismatch. Ideally, the conjugate would remain intact while rhodium ferried the platinum subunit towards mismatches, followed by hydrolysis and platination of mismatched DNA. Again, this complex displayed no cell-selective targeting of MMR-deficiency, although it also did not display a preference for the MMR-proficient line. Additionally, this conjugate exhibited similar levels of platination in both mismatched and well-matched DNA *in vitro*.[26]

In our latest efforts to develop selective bifunctional conjugates, we turn to a new family of metalloinsertor complexes, developed and characterized only in the last two years. Each complex in this new generation of metalloinsertors contains an unusual ligand coordination involving a Rh—O bond. In all cases, a tris-heteroleptic Rh(III) center employs the inserting chrysi ligand, a 1,10-phenanthroline (phen) non-inserting ancillary ligand, and a 2-pyridylethanol ligand that forms an *N,O*-chelate. In this family of metalloinsertors, the hydroxyl group coordinates the Rh(III) center as an X-type ligand, reducing the overall charge of the complex from [3+] to [2+]. As a result, the pK_a of the chrysi immines, normally singly deprotonated when bound to DNA, is increased

above biological pH, leading to a puckering of the ligand. An alternate mode of metalloinsertion has previously been proposed to accommodate these distortions in structure. These complexes also exhibit unprecedented potency (IC_{50} = 300 nM, where IC_{50} represents the concentration at which 50% of the cells are viable) in MMR-deficient cells, while maintaining excellent cell-selectivity, making them promising new scaffolds for conjugate design.[24]

The original complex in this family, $[Rh(chrysi)(phen)(DPE)]^{2+}$, (**Figure 4.1**) contains a 1,1-di(pyridin-2-yl)ethanol (DPE) ligand that was originally intended to chelate via both pyridine rings to afford the all-nitrogen coordination environment observed for earlier generations of metalloinsertors.[22] The hydroxyl group was included as a moiety that could potentially be functionalized for conjugation. It was only after structural characterization of the complex through X-ray crystallography that the true binding mode was revealed. It was later found that a number of functional groups could be introduced into this ligand structure in place of the extraneous pyridine without sacrificing DNA binding ability, cell-selectivity, or potency.[24] Here, we sought to develop the first generation conjugate derived from this new family, through coordination of the "dangling" pyridine to a second metal center. This pyridine still represents a viable chelating environment that could be exploited to confer selectivity onto other inorganic therapeutic cargo, such as *cis*-platinum anticancer agents. We have synthesized a new bifunctional metalloinsertor complex, wherein a cisplatin group is attached to $[Rh(chrysi)(phen)(DPE)]^{2+}$ via coordination to the extraneous pyridine. This conjugate,

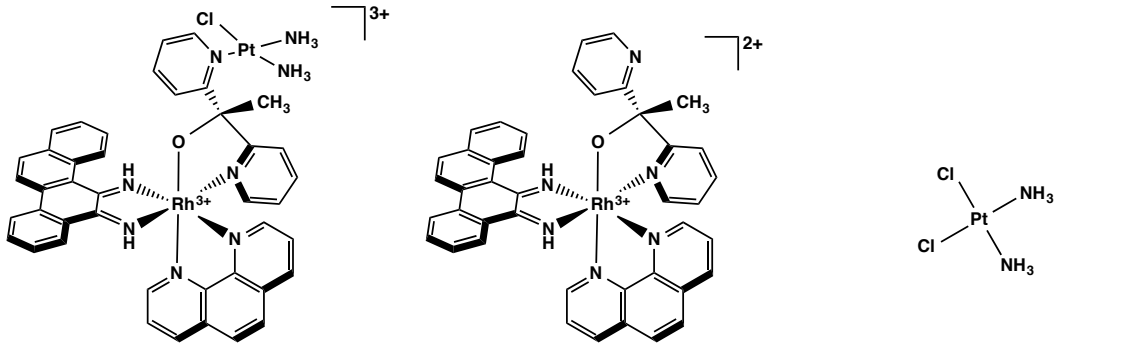

rac-[Rh(chrysi)(phen)(DPE-Pt(NH_3)$_2$Cl)]$^{3+}$ *rac*-[Rh(chrysi)(phen)(DPE)]$^{2+}$ *cis*-dichlorodiammineplatinum (II)

Figure 4.1 Chemical structures of complexes studied. [Rh(chrysi)(phen)(DPE-Pt(NH_3)$_2$Cl]$^{3+}$ (left) is a bifunctional comprised of a trisheteroleptic rhodium metalloinsertor, which recognizes DNA mismatches, tethered to a *cis*-platinum (II) anticancer agent, which forms covalent adducts with DNA. [Rh(chrysi)(phen)(DPE)]$^{2+}$ (center) is the rhodium metalloinsertor parent complex, which contains an unusual Rh—O axial coordination that contributes to its enhanced efficacy. *Cis*-dichlorodiammineplatinum (II) (right) is the FDA-approved chemotherapeutic known as cisplatin.

$[Rh(chrysi)(phen)(DPE\text{-}Pt(NH_3)_2Cl)]^{3+}$ (**Figure 4.1**), preferentially targets platinum to mismatched DNA *in vitro* and forms unusual, nonclassical covalent adducts.

4.2 Experimental

4.2.1 Materials

A2780cis cells, cisplatin, and all organic reagents were purchased from Sigma-Aldrich unless otherwise noted. Commercially available chemicals were used as received without further purification. $RhCl_3$ starting material was purchased from Pressure Chemical Co (Pittsburgh, PA). Sep-pak C_{18} solid-phase extraction (SPE) cartridges were purchased from Waters Chemical Co. (Milford, MA). Media and supplements were purchased from Invitrogen (Carlsbad, CA). BrdU, antibodies, and buffers were purchased in kit format from Roche Molecular Biochemical (Mannheim, Germany).

Oligonucleotides were ordered from Integrated DNA Technologies and purified by HPLC using a C18 reverse-phase column (Varian, Inc; Corona, CA). All HPLC purifications were carried out on a Hewlett-Packard 1100 HPLC. DNA purity was confirmed by MALDI-TOF mass spectrometry and quantified by UV-visible spectroscopy (UV-vis) using the extinction coefficients at 260 nm estimated for single-stranded DNA. UV-vis characterizations were performed on a Beckmann DU 7400 spectrophotometer. Radiolabeled [^{32}P]-ATP was purchased from MP Biomedicals (Santa Ana, CA).

The syntheses of chrysene-5,6-dione (chrysi), 1,1-di(pyridin-2-yl)ethanol (DPE), and $[Rh(chrysi)(phen)(DPE)]^{2+}$ were carried out according to published procedures.[22,28,29]

4.2.2 Synthesis of $[Rh(chrysi)(phen)(DPE\text{-}Pt(NH_3)_2Cl)]^{3+}$ (Scheme 4.1)

A 250 ml round bottomed flask was charged with [Rh(chrysi)(phen)(DPE)]TFA_2 (272 mg, 0.28 mmol) (prepared according to literature procedures) and cisplatin (305 mg, 1 mmol, 3.57 equiv) in 100 ml H_2O. One drop of concentrated HCl was added, and the solution was stirred at reflux for an additional 48 h. The reaction was hot-filtered through a medium glass frit and purified by reverse-phase HPLC (85:15:0.1 to 40:60:0.1 H_2O/MeCN/TFA gradient). Fractions were pooled and dried *in vacuo* to afford the bimetallic product as a red-brown solid. To obtain the complex as the chloride salt, [Rh(DPE)Pt]TFA_3 was redissolved in 50 mM $HCl_{(aq)}$ and freeze-dried under high vacuum. This process was repeated three times until the TFA counterion was eliminated. Yield: 60 mg (16% by HPLC). ^{1}H NMR (500 MHz, D_2O): δ 9.39 (d, J = 5.3 Hz, 1H), 8.95 (d, J = 8.0 Hz, 1H), 8.90 (d, J = 6.7 Hz, 2H), 8.87 – 8.68 (m, 1H), 8.49 – 8.35 (m, 1H), 8.34 – 8.27 (m, 1H), 8.24 – 8.18 (m, 1H), 8.14 – 8.11 (m, 1H), 8.07 (d, J = 10.3 Hz, 1H), 8.03 (s, 1H), 8.00 (d, J = 6.7 Hz, 2H), 7.96 (d, J = 8.0 Hz, 2H), 7.90 (d, J = 7.9 Hz, 1H), 7.81 (s, 1H), 7.72 (d, J = 7.5 Hz, 1H) 7.68 – 7.60 (m, 1H), 7.57 (s, 1H), 7.52 (t, J = 7.5 Hz, 1H), 7.41 (s, 2H), 7.32 (d, J = 6.8 Hz, 2H), 7.27 – 7.17 (m, 1H), 7.00 (d, J = 7.8 Hz, 1H), 3.66 – 3.59 (m, 3H), 3.54 (dd, J = 5.6, 3.5 Hz, 3H), 2.95 (s, 3H). ESI-MS (cation, **Figure 4.2**): *m/z* calc 1003.251, obs. 1001.8 ($M - 2H^+$). UV-vis (H_2O, pH 7.0): 270 nm (134,700 M^{-1} cm^{-1}), 303 nm (72,400 M^{-1} cm^{-1}), 442 nm (19,200 M^{-1} cm^{-1}), 581 nm (10,600 M^{-1} cm^{-1}).

4.2.3 Photocleavage Competition Titrations

A single-stranded DNA oligomer with the sequence 5*'-TTAGGATCATCCATATA-3' (underline denotes the mismatch, asterisk denotes the radiolabel) was labeled at the 5'-end with [^{32}P]-ATP as described in **Section 4.2.3** and

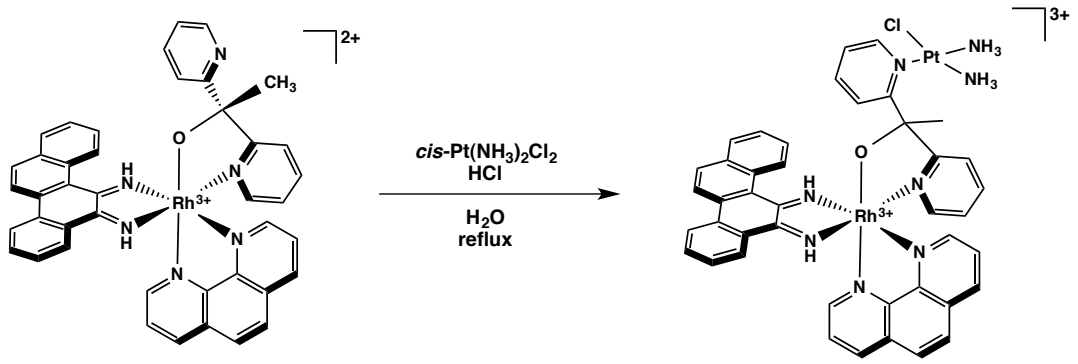

Scheme 4.1 Synthesis of $[Rh(chrysi)(phen)(DPE\text{-}Pt(NH_3)_2Cl]^{3+}$

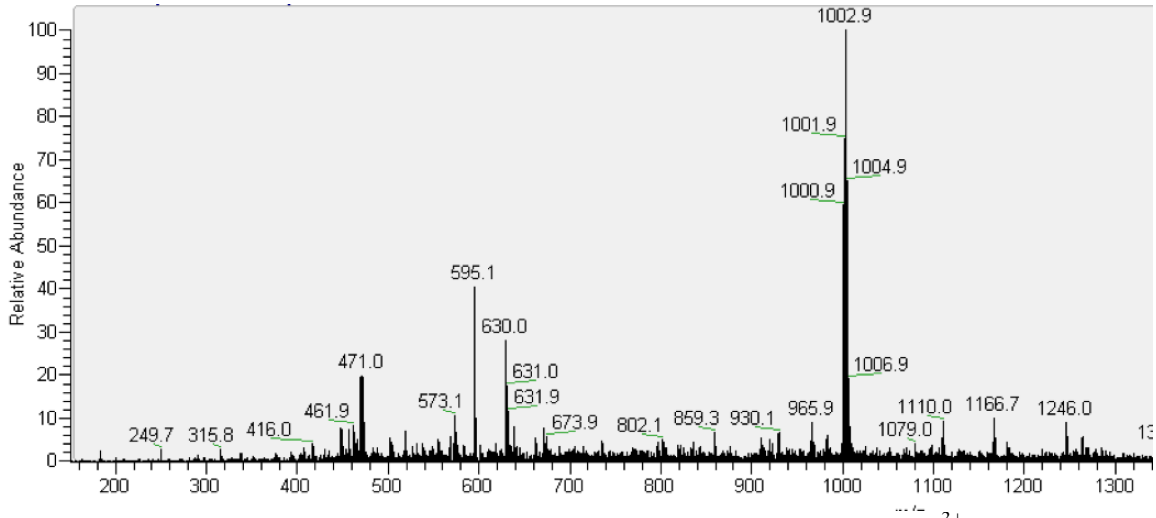

Figure 4.2 ESI-MS spectrum of $[Rh(chrysi)(phen)(DPE\text{-}Pt(NH_3)_2Cl]^{3+}$; *m/z* = 1000.9 – 1006.9 (indicative of the Rh and Pt isotope patterns), calc 1003.251.

annealed with a complement containing a CC mismatch at the position indicated. Racemic solutions of $[Rh(chrysi)(phen)(DPE\text{-}Pt(NH_3)_2Cl)]^{3+}$ were prepared in Milli-Q water over a range of concentrations (100 nM – 50 μM). For each sample, 4 μM *rac*-$[Rh(bpy)_2chrysi]Cl_3$ (5 μl), which photocleaves DNA at mismatched sites, 2 μM annealed mismatched duplex DNA (10 μl), and the non-photocleaving competitor complex at various concentrations (5 μl) were combined to give 1 μM *rac*-$[Rh(bpy)_2chrysi]Cl_3$, 1 μM duplex DNA, and 75 mM $NaCl_{(aq)}$ as the final concentrations. Samples were irradiated on an Oriel (Darmstadt, Germany) 1000-W Hg/Xe solar simulator (340-440 nm) for 15 min, incubated at 37 °C for 10 min, and dried *in vacuo*. The irradiated samples were electrophoresed on a 20% denaturing polyacrylamide gel and exposed to a phosphor screen. The amounts of DNA in each band were analyzed by autoradiography and quantitated by phosphorimagery (ImageQuant).

4.2.4 Binding Constant Determination

As the $[Rh(chrysi)(phen)(DPE\text{-}Pt(NH_3)_2Cl)]^{3+}$ complex does not photocleave DNA upon irradiation, the binding affinity for a CC mismatch was determined *via* a competition titration against *rac*-$[Rh(bpy)_2chrysi]^{3+}$, which does photocleave DNA at mismatched sites. To assess the binding of the rhodium subunit of $[Rh(chrysi)(phen)(DPE\text{-}Pt(NH_3)_2Cl)]^{3+}$ at the CC mismatch, the fraction of cleaved DNA was quantified and expressed as a percentage of the total DNA in each lane and plotted against the log of the concentration of $[Rh(chrysi)(phen)(DPE\text{-}Pt(NH_3)_2Cl)]^{3+}$. The data from three independent titration experiments were each fit to a sigmoidal curve using OriginPro 8.5. The concentration of rhodium at the inflection point at the curve ($[Rh_{50\%}]$) was then used to solve simultaneous equilibria involving DNA, $[Rh(bpy)_2chrysi]Cl_3$, and

[Rh(chrysi)(phen)(DPE-Pt(NH_3)$_2$Cl)]$^{3+}$ in Mathematica 8.0 to obtain the binding constant (K_B).

DNA platination was analyzed in a similar manner, wherein the fraction of platinated DNA was quantified and expressed as a percentage of the total DNA in each lane

4.2.5 Platinum Binding to Mismatched and Well-Matched Duplex DNA

A single-stranded DNA oligomer with the sequence 5*'-TTAGGATCATCCATATA-3' (underline denotes the mismatch, asterisk denotes the radiolabel) was labeled at the 5'-end with [^{32}P]-ATP and polynucleotide kinase (PNK) at 37 °C for 2 h. The radiolabeled DNA was purified by gel electrophoresis and annealed to either its mismatched complement (containing a CC mismatch) or a fully matched complement strand by heating to 90 °C in buffer (100 mM NaCl, 20 mM NaP_i, pH 7.1), followed by slow cooling to ambient temperature over 2 h, to give a final concentration of 2 μM duplex DNA. Racemic solutions of [Rh(chrysi)(phen)(DPE-Pt(NH_3)$_2$Cl)]$^{3+}$ were prepared in 50 mM $NaCl_{(aq)}$ over a range of concentrations (100 nM – 5 μM). For each sample, 2 μM annealed mismatched duplex DNA (10 μl) was mixed with [Rh(chrysi)(phen)(DPE-Pt(NH_3)$_2$Cl)]$^{3+}$ at various concentrations (10 μl) to give 1 μM duplex DNA and 75 mM $NaCl_{(aq)}$ as the final concentrations. A "light" control, (ØRh, ØPt) consisting of 2 μM DNA mixed with 10 μl Milli-Q water, and a "dark" control (Ø *hυ*), containing the DNA mixed with the highest concentration of competitor complex without irradiation, were also prepared. The samples were incubated at 37 °C for periods of 1, 3, or 18h to promote the formation of the platinated DNA adducts. After the incubation period, samples were quenched with 50 μl of 0.1 M $NaCl_{(aq)}$ and cooled to 4

°C for 30 min. Except for the dark controls, samples were irradiated on an Oriel (Darmstadt, Germany) 1000-W Hg/Xe solar simulator (340-440 nm) for 15 min and dried *in vacuo*. The irradiated samples were electrophoresed on a 20% denaturing polyacrylamide gel and exposed to a phosphor screen. The amounts of DNA in each band were analyzed by autoradiography and quantitated by phosphorimagery (ImageQuant).

4.2.6 Dimethyl Sulfate Footprinting of Platinated DNA

DNA footprinting of guanine by dimethyl sulfate (DMS) was carried out according to literature procedures.[30] Briefly, single stranded DNA with the sequence 5'-TTAGGATCATCCATATA-3' (underline denotes the mismatch) was labeled at the 5'-end with [^{32}P]-ATP and annealed with its CC mismatched complement as described above. A solution of 1 μM annealed DNA was platinated with either [Rh(chrysi)(phen)(DPE-Pt(NH_3)$_2$Cl)]$^{3+}$ (1 or 5 μM) or cisplatin (1 μM) by incubation at 37 °C for 90 min. The platination reaction was quenched via addition of 0.1 M $NaCl_{(aq)}$ followed by cooling to 4 °C for 30 min. Samples were purified by ethanol precipitation and dried *in vacuo.* The samples were taken up in 5 μl Milli-Q water, diluted with DMS buffer (50 mM sodium cacodylate, 1 mM EDTA, pH 7.5), and 2 mM calf-thymus DNA (4 μl) was added as a carrier DNA. Samples were cooled to 0 °C and treated with 5 μl DMS (10% v/v in EtOH, prepared immediately before use) for 5 min at 25 °C. The reaction was quenched *via* addition of the DMS stop solution (1.5 M NaOAc, 1 M β-mercaptoethanol, 250 μg/ml yeast tRNA) at 0 °C. Following ethanol precipitation of the DNA, samples were treated with 10% aqueous piperidine and heated to 90 °C for 30 min. The piperidine was removed *in vacuo*, and samples were electrophoresed on a 20% denaturing polyacrylamide gel and exposed to a phosphor screen. The amounts of DNA

in each band were analyzed by autoradiography and quantitated by phosphorimagery (ImageQuant).

4.2.7 Cell Culture

4.2.7.1 HCT116N/O. HCT116N (MMR-proficient) and HCT116O (MMR-deficient) cells were grown in RPMI medium 1640 supplemented with 10% fetal bovine serum, 400 μg/ml Geneticin (G418), 2 mM L-glutamine, 0.1 mM nonessential amino acids, 1 mM sodium pyruvate, 100 units/ml penicillin, and 100 μg/ml streptomycin. Cells were grown in tissue culture flasks (Corning Costar, Acton, MA) at 37 °C under a humidified atmosphere (5% CO_2).

4.2.7.2 A2780cis. A2780cis cells (Sigma-Aldrich Co.) were grown in RPMI medium 1640 supplemented with 105 fetal bovine serum, 200 mM L-glutamine, 100 units/ml penicillin, and 100 μg/ml streptomycin. To retain resistance, cisplatin was added to the media every 2-3 passages to a final concentration of 1 μM. Cells were grown in tissue culture flasks (Corning Costar, Acton, MA) at 37 °C under a humidified atmosphere (5% CO_2).

4.2.8 MTT Cytotoxicity Assay

The cytotoxic effects of conjugate $[Rh(chrysi)(phen)(DPE\text{-}Pt(NH_3)_2Cl)]^{3+}$, $[Rh(chrysi)(phen)(DPE)]^{2+}$, and cisplatin were studied *via* MTT (3-(4,5-dimethylthiazol-2-yl)-2,5-diphenyltetrazolium bromide) assay in the cisplatin-resistant A2780cis, MMR-proficient HCT116N, and MMR-deficient HCT116O cell lines.[31] For biological experiments, $[Rh(chrysi)(phen)(DPE\text{-}Pt(NH_3)_2Cl)]^{3+}$ and cisplatin were prepared in saline solution (20 mM NaCl), and $[Rh(chrysi)(phen)(DPE)]^{2+}$ was dissolved in deionized water. Cells were plated in 96-well plates at 50,000 cells/well and incubated with varying

concentrations of metal complex for 72h under humidified atmosphere. After the incubation period, MTT was added, and the cells were incubated for an additional 4 h. The resulting formazan crystals were solubilized over a period of 24 h at 37 °C, 5% CO_2. Formazan formation was quantified *via* electronic absorption at 550-600 nm with a reference wavelength of 690 nm. Cell viability is expressed as a function of formazan formation and normalized to that of untreated cells. Standard errors were calculated from 5 replicates.

4.2.9 MTT Caspase and PARP Inhibition Assays

The cytotoxic effects of conjugate $[Rh(chrysi)(phen)(DPE\text{-}Pt(NH_3)_2Cl)]^{3+}$ and cisplatin were studied *via* MTT (3-(4,5-dimethylthiazol-2-yl)-2,5-diphenyltetrazolium bromide) assay in the HCT116O and HCT116N cell lines. Cells were plated in 96-well plates at 50,000 cells/well and incubated with 0 or 5 μM of metal complex. For caspase-inhibition assays, Z-VAD-FMK was added to a final concentration of 35 μM. For poly-ADP ribose polymerase (PARP) assays, the inhibitor 3,4-dihydro-5[4-(1-piperindinyl)butoxy]-1(2*H*)-isoquinoline (DPQ) was added to a final concentration of 50 μM. Controls wherein cells were treated with inhibitor alone in the absence of metal complex were included. Cells were incubated under humidified atmosphere for 72 h and labeled with MTT for an additional 4 h at 37 °C, 5% CO_2. The ensuing formazan crystals were dissolved with a lysis buffer (10% SDS in 10 mM HCl) according to the manufacturer's instructions. MTT reduction to formazan was quantified by electronic absorption at 570 nm (background: 690 nm), and percent viability was expressed as the amount of formazan in treated cells compared to that of the untreated controls.

4.3 Results

4.3.1 DNA Binding Studies

The rhodium mismatch recognition and covalent platinum binding of DNA were analyzed with mismatched and well-matched DNA oligomers with the sequence on 20% denaturing PAGE gels. Although mismatch recognition and platinum adduct formation can be visualized simultaneously under the same conditions (**Figure 4.3**), platinum binding is optimally observed under saline conditions (75-100 mM $NaCl_{(aq)}$). While this affords thermodynamic control over the DNA platination reaction, thereby enhancing selective platination of mismatched DNA, high salt concentrations make quantification of photocleavage at the mismatched site challenging. As a result, metalloinsertion at the mismatch was analyzed separately from platination of mismatched and well-matched DNA, under aqueous conditions.

4.3.1.1 Binding Affinity of Rhodium at a CC Mismatch

In vitro DNA binding studies were performed with racemic aqueous solutions of $[Rh(chrysi)(phen)(DPE\text{-}Pt(NH_3)_2Cl)]^{3+}$ and radiolabeled hairpin DNA containing a CC mismatch with the sequence 5*′-GGCAGGCATGGCTTTTTGCCATCCCTGCC-3′ (underline denotes the mismatch; asterisk denotes the radiolabel) Single-stranded DNA was labeled at the 5'-end with [^{32}P]-ATP and polynucleotide kinase (PNK) at 37 °C for 2h as described above. The conjugate was bound with mismatched hairpin DNA at varying concentrations and irradiated (340-440 nm) for 15 min. Samples were then incubated at 37 °C for 10 min and electrophoresed on a 20% denaturing PAGE gel. As $[Rh(chrysi)(phen)(DPE\text{-}Pt(NH_3)_2Cl)]^{3+}$ does not cleave DNA upon irradiation, a competition titration was carried out using $[Rh(bpy)_2chrysi]^{3+}$, which does photocleave DNA at the site of a mismatch.[10] The conjugate inhibits photocleavage by *rac*-

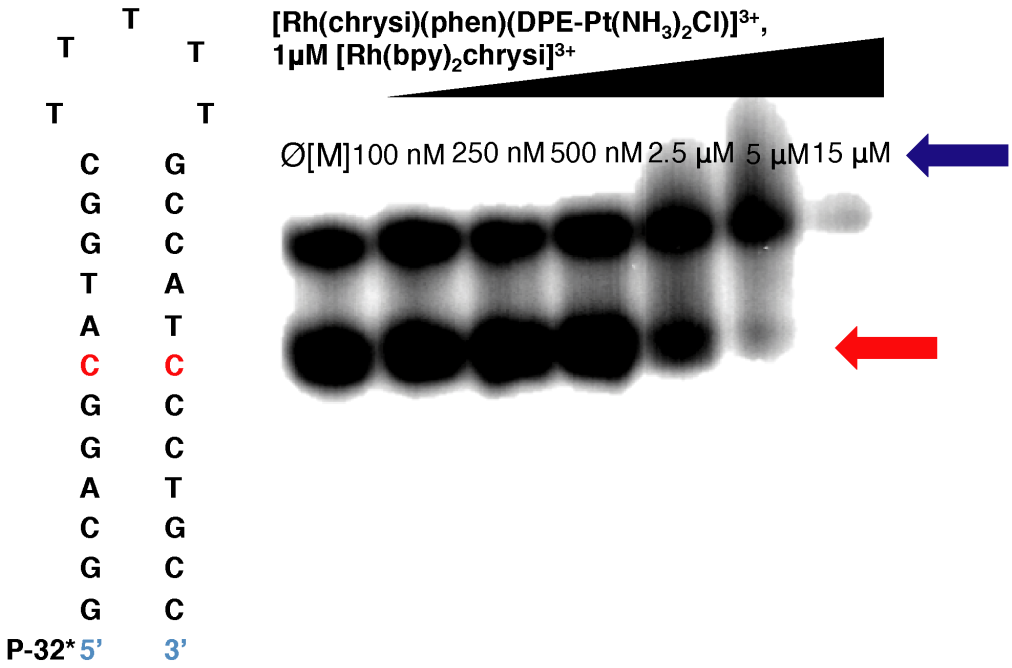

Figure 4.3 Competition titration of increasing concentrations of $[Rh(chrysi)(phen)(DPE\text{-}Pt(NH_3)_2Cl)]^{3+}$ (0-15 μM) with 1 μM *rac*-$[Rh(bpy)_2chrysi]^{3+}$ on 1 μM 5’-[^{32}P] labeled 29mer hairpin DNA of the sequence indicated containing a CC mismatch (denoted in red). Samples were irradiated (340-440 nm) for 15 min and electrophoresed on a 20% denaturing polyacrylamide gel. Controls without Rh were included (Ø[M]). $[Rh(chrysi)(phen)(DPE\text{-}Pt(NH_3)_2Cl)]^{3+}$ inhibits photocleavage by $[Rh(bpy)_2chrysi]^{3+}$ at the mismatched site. The site of photocleavage by $[Rh(bpy)_2chrysi]^{3+}$ at the mismatch is indicated by a red arrow at bands located below the unmodified parent band. Bands of reduced electrophoretic mobility, located above the unmodified parent DNA and indicated by a blue arrow, are indicative of covalent binding by the platinum subunit.

$[Rh(bpy)_2chrysi]^{3+}$ at the mismatched site in a dose-dependent manner (**Figure 4.3**); this indicates that the complex binds specifically to the mismatch *via* metalloinsertion. Experimental conditions were carried out to minimize platinum adduct formation, thus limiting interference of covalent platinum binding on the equilibrium binding constant of the rhodium subunit at the mismatch. Nevertheless, some platinum binding is observed to occur simultaneously with mismatch binding, as indicated by the presence of slowly migrating bands located above the unmodified parent band. This result suggests that the complex is capable of binding mismatched DNA bifunctionally, through simultaneous metalloinsertion at the mismatched site as well as the formation of covalent platinum crosslinks. The amount of photocleaved DNA was quantified and plotted against the logarithmic concentration of the complex (log[RhPt]), and the K_B value of RhPt was calculated by solving simultaneous equilibria at the inflection point of the titration curve (**Figure 4.4**). The binding affinity of RhPt for a CC mismatch was determined to be 4.8 x 10^6 M^{-1}, comparable to that of monomeric metalloinsertors.[20,22,23]

4.3.1.2 Platination of Mismatched and Well-Matched DNA

The formation of platinum-DNA crosslinks was analyzed *in vitro* via gel electrophoresis. Dissociation of the labile chloride ligand from the platinum center in solution enables the formation of covalent platinum adducts with DNA. The reaction between the conjugate and mismatched (CC) and well-matched duplex DNA oligomers was analyzed as a function of incubation time at 37 °C as well as complex concentration.

A time-course experiment was used to explore the formation of Pt-DNA adducts with radiolabeled duplex DNA of the sequence 5*'-TTAGGATCATCCATATA-3' (underline denotes the site of a CC mismatch, asterisk denotes the radiolabel) annealed

with either its mismatched or fully matched complement strands. Racemic mixtures of $[Rh(chrysi)(phen)(DPE\text{-}Pt(NH_3)_2Cl)]^{3+}$ (1 μM) and mismatched or well-matched DNA (1 μM) were incubated in buffer (75 mM NaCl, 10 mM NaP_i, pH 7.1) at 37 °C for periods of either 1, 3, or 18 h. After the incubation period, samples were quenched with 0.1 M $NaCl_{(aq)}$, cooled to 4 °C, and electrophoresed on a 20% denaturing PAGE gel. Platination of the DNA is indicated by the appearance of bands with reduced electrophoretic mobility, located above the unmodified parent bands in the autoradiogram.

The resulting autoradiogram is shown in **Figure 4.5**. The $[Rh(chrysi)(phen)(DPE\text{-}Pt(NH_3)_2Cl)]^{3+}$ conjugate exhibits a clear preference for mismatched DNA over fully matched oligomers after 1 and 3 hr incubation periods. The 18h incubations resulted in complete degradation of the DNA, and the bands could not be observed above background.

The amount of platinated DNA was quantified as a fraction of the total DNA in each sample (**Figure 4.6**). At incubation periods of 1 and 3 hours, platination of mismatched DNA over well-matched is enhanced by 20% and 17%, respectively. At 1h, 61% of mismatched DNA contains covalent platinum adducts, compared to 41% of fully matched DNA. Longer incubation (3h) results in a slight decrease in the differential platination of mismatched over well-matched DNA (56% versus 39%, respectively). Samples incubated for 18 h were not quantified.

DNA platination was also analyzed in a dose-dependent manner, as can be seen in **Figure 4.7**. Racemic mixtures of $[Rh(chrysi)(phen)(DPE\text{-}Pt(NH_3)_2Cl)]^{3+}$ (0.1 – 5 μM) and mismatched or well-matched DNA (1 μM) were incubated at 37 °C for 2h and

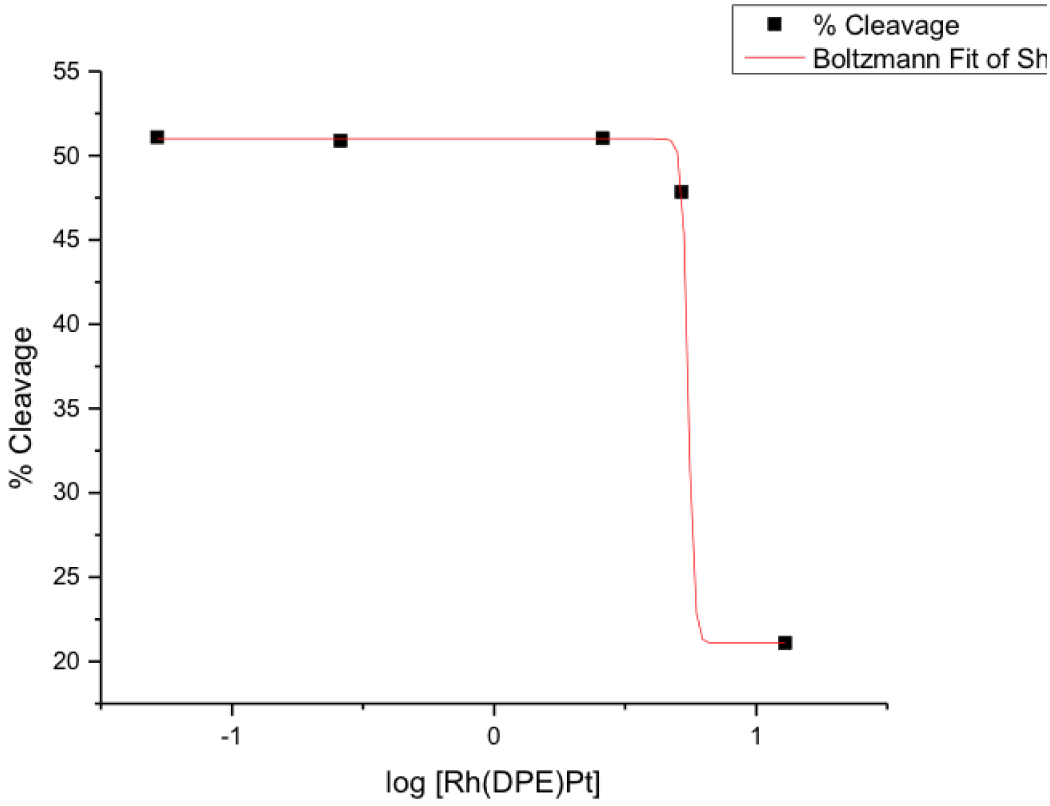

Figure 4.4 Representative sigmoidal curve (Boltzmann fit) of photocleavage competition titrations of $[Rh(chrysi)(phen)(DPE\text{-}Pt(NH_3)_2Cl)]^{3+}$ for binding constant determination at the CC mismatch. K_B was calculated by solving simultaneous equilibria at the inflection point of the curve. Experiments were conducted in buffer (50 mM NaCl, 10 mM NaP_i, pH 7.1) using 1 μM hairpin DNA and 1 μM rac-$[Rh(bpy)_2chrysi]^{3+,}$ with 0-15 μM $[Rh(chrysi)(phen)(DPE\text{-}Pt(NH_3)_2Cl)]^{3+}$competitor complex.

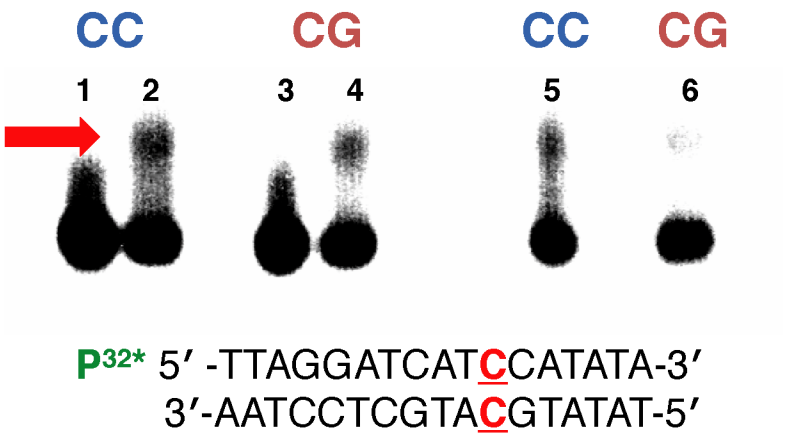

Figure 4.5 Autoradiogram depicting the formation of covalent platinum adducts with mismatched and well-matched DNA duplexes (1 μM) as a function of time. $[Rh(chrysi)(phen)(DPE\text{-}Pt(NH_3)_2Cl)]^{3+}$ (1 μM) was incubated with 5'end radiolabeled duplex DNA of the sequence indicated (bottom; the site of the CC mismatch is denoted in red) as well as the corresponding well-matched duplex in buffer (75 mM NaCl, 10 mM NaP_i, pH 7.1) at 37 °C for 1, 3, or 18h. Samples were irradiated for 15 min and electrophoresed on a 20% denaturing PAGE gel. Platinum crosslinking of DNA is indicated by the appearance of slow-moving bands located above the unmodified parent DNA; platinated DNA is denoted by a red arrow. Lanes: (1) untreated duplex DNA containing a CC mismatch; (2) mismatched DNA incubated with metal complex for 1h; (3) untreated well-matched DNA; (4) well-matched DNA incubated with metal complex for 1h; (5) mismatched DNA treated with metal complex for 3h; (6) well-matched DNA treated with metal complex for 3h. Samples treated with metal complex for 18h were degraded on the gel and are not visible in the autoradiogram.

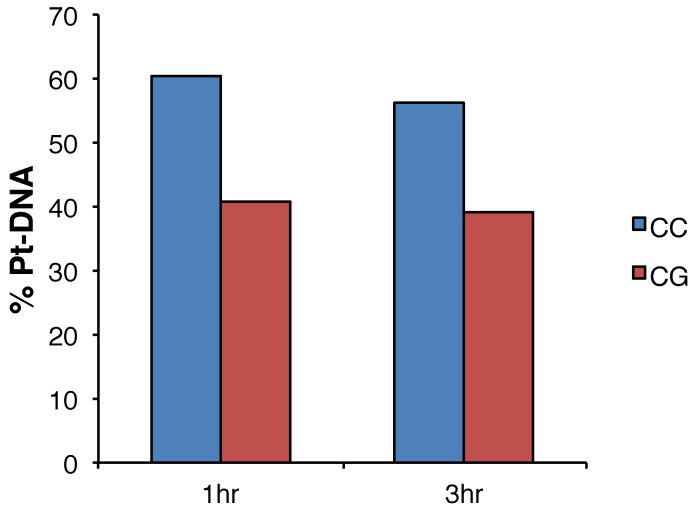

Figure 4.6 Quantification of platination of mismatched (CC, blue) and well-matched (CG, red) duplex DNA (1 μM) by $[Rh(chrysi)(phen)(DPE\text{-}Pt(NH_3)_2Cl)]^{3+}$ (1 μM). Samples were incubated at 37 °C for 1, 3, or 18h and electrophoresed on a 20% denaturing PAGE gel. The amount of platinated DNA (% Pt-DNA) is expressed as a fraction of the total DNA in each sample. Samples heated for 18h were degraded and not quantified.

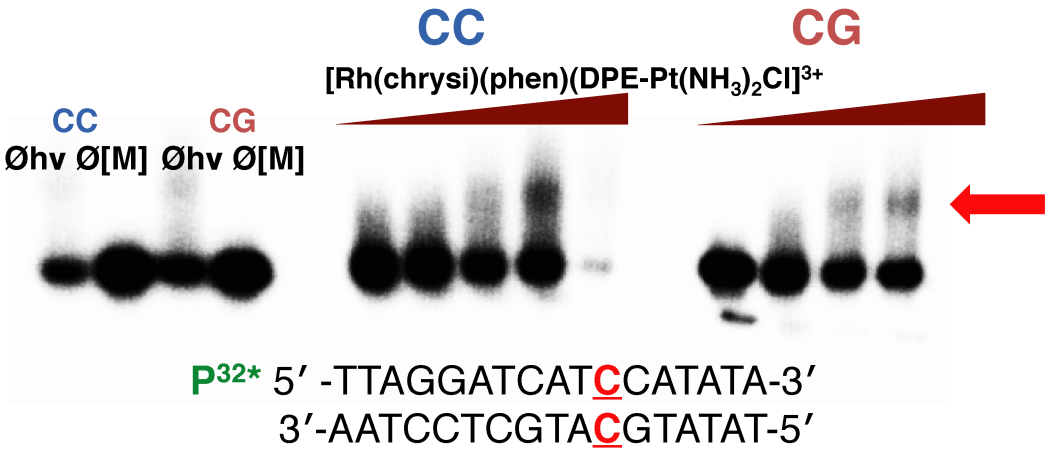

Figure 4.7 Autoradiogram depicting the formation of covalent platinum adducts with mismatched and well-matched DNA duplexes (1 μM) as a function of metalloinsertor concentration. $[Rh(chrysi)(phen)(DPE\text{-}Pt(NH_3)_2Cl)]^{3+}$ (100 nM – 5 μM) was incubated with 5'end radiolabeled duplex DNA of the sequence indicated (bottom; the site of the CC mismatch is denoted in red) as well as the corresponding well-matched duplex in buffer (75 mM NaCl, 10 mM NaP_i, pH 7.1) at 37 °C for 2h. Samples were irradiated for 15 min and electrophoresed on a 20% denaturing PAGE gel. Controls without irradiation (Øhν) and without metal complex (Ø[M]) were included for each type of DNA (mismatched DNA is denoted by "**CC**" in blue; well-matched DNA is denoted by "**CG**" in red) and are depicted on the left. Platinum crosslinking of DNA is indicated by the appearance of slow-moving bands located above the unmodified parent DNA; platinated DNA is denoted by a red arrow. Platination of mismatched DNA is shown in the center (denoted by "**CC**" in blue, and platination of well-matched DNA is shown on the right (denoted by "**CG**" in red).

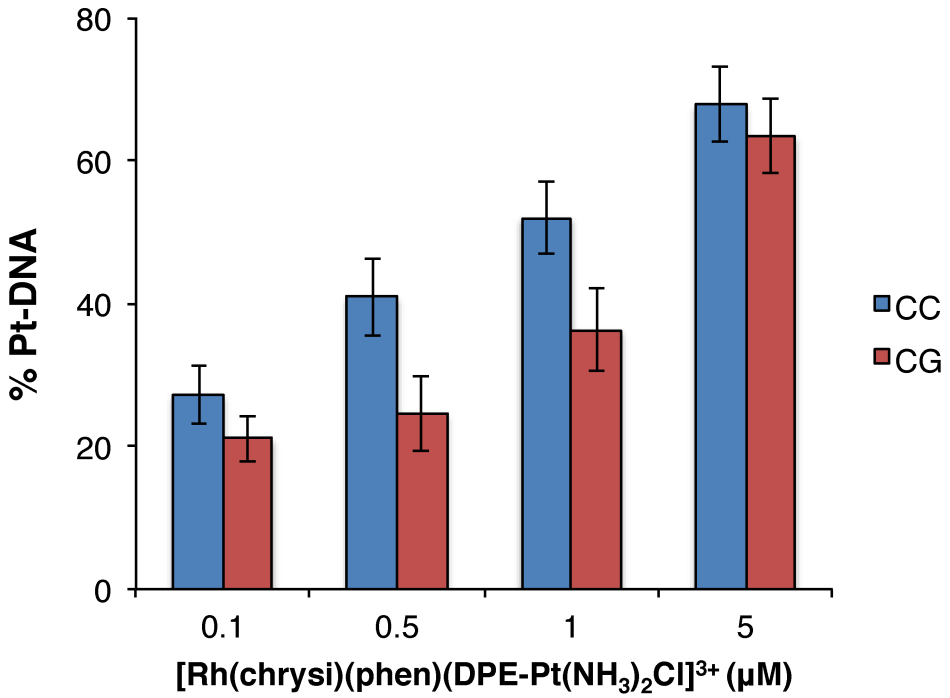

Figure 4.8 Quantification of platination of mismatched (CC, blue) and well-matched (CG, red) duplex DNA (1 μM) by $[Rh(chrysi)(phen)(DPE\text{-}Pt(NH_3)_2Cl)]^{3+}$ (0.1 – 5 μM). Samples were incubated at 37 °C for 2h and electrophoresed on a 20% denaturing PAGE gel. The amount of platinated DNA (% Pt-DNA) is expressed as a fraction of the total DNA in each sample.

electrophoresed on a 20% denaturing polyacrylamide gel. The platinum-DNA bands were quantified by autoradiography, shown in **Figure 4.8**, revealing a preference for mismatched DNA at low concentrations (0.1 – 1 μM) of conjugate. At 500 nM $[Rh(chrysi)(phen)(DPE\text{-}Pt(NH_3)_2Cl)]^{3+}$, 41 ± 5.4% of mismatched duplex contains platinum adducts versus 25 ± 5.3% of well-matched DNA. Optimal selectivity is achieved at stoichiometric Pt:DNA (1 μM), with 52 ± 5.1% platinated mismatched DNA versus 36 ± 5.7% ($p < 0.05$ by unpaired two-tailed *t* test). Unsurprisingly, this differential platinum binding diminishes at high concentrations of the complex, and mismatched and well-matched DNA is platinated equally; 72% and 70% platination of mismatched and well-matched DNA is observed, respectively. It would appear as though the formation of platinum crosslinks is guided at least in part by mismatch recognition by the rhodium subunit.

4.3.1.3 Dimethyl Sulfate Footprinting of Pt-DNA Crosslinks

To probe the potential site of platinum adduct formation, dimethyl sulfate (DMS) footprinting was carried out for platinated mismatched and well-matched DNA duplexes. Typically, the preferential binding site of platinum is the *N*7 position of guanine; DMS methylation at guanine *N*7 induces cleavage of the DNA at these residues.[30] The degree of DMS-induced guanine cleavage indicates whether platinum is coordinated. Uncoordinated guanines will incur relatively high levels of cleavage upon DMS treatment, while platinated sites will be protected. Duplex DNA (1 μM) containing a single CC mismatch, as well as a similarly well-matched sequence (see **Section 4.3.1.2** for sequence) was radiolabeled at the 5'-end with [^{32}P] and incubated with either cisplatin (1 μM) or $[Rh(chrysi)(phen)(DPE\text{-}Pt(NH_3)_2Cl)]^{3+}$ (1 or 5 μM) for 90 min at 37 °C to

promote the formation of Pt-DNA adducts; untreated controls of mismatched and well-matched DNA were also included. The DNA was then purified and subjected to treatment with 10% DMS, followed by cleavage by piperidine (1 M) and denaturing gel electrophoresis (20% polyacrylamide).

The resulting autoradiogram is shown in **Figure 4.9**. The cleavage products of the two guanine residues in the radiolabeled strand are indicated by bands of high electrophoretic mobility located below the unmodified parent bands. For both mismatched and well-matched DNA, treatment with [Rh(chrysi)(phen)(DPE-$Pt(NH_3)_2Cl$)]$^{3+}$ conjugate does not confer protection of the guanine residues from DMS methylation and cleavage. In fact, a marked *increase* in guanine cleavage product is observed with conjugate-bound DNA at both 1 and 5 μM treatment, compared to untreated and cisplatin-treated DNA. Furthermore, this increase is observed for both guanine residues, which occur consecutively in the sequence. However, the conjugate clearly forms covalent adducts, as is indicated by the presence of slow-migrating bands located above the unmodified parent bands. The [Rh(chrysi)(phen)(DPE-$Pt(NH_3)_2Cl$)]$^{3+}$ complex does not coordinate at the expected guanine sites; rather, the alternative platinum binding site likely results in a conformational change to the DNA that enhances the accessibility of both guanine residues to methylation by DMS.

4.3.2 MTT Cytotoxicity Assay

The cytotoxic effects of [Rh(chrysi)(phen)(DPE-$Pt(NH_3)_2Cl$)]$^{3+}$ were probed via MTT cytotoxicity assay (MTT = (3-(4,5-dimethylthiazol-2-yl)-2,5-diphenyltetrazolium

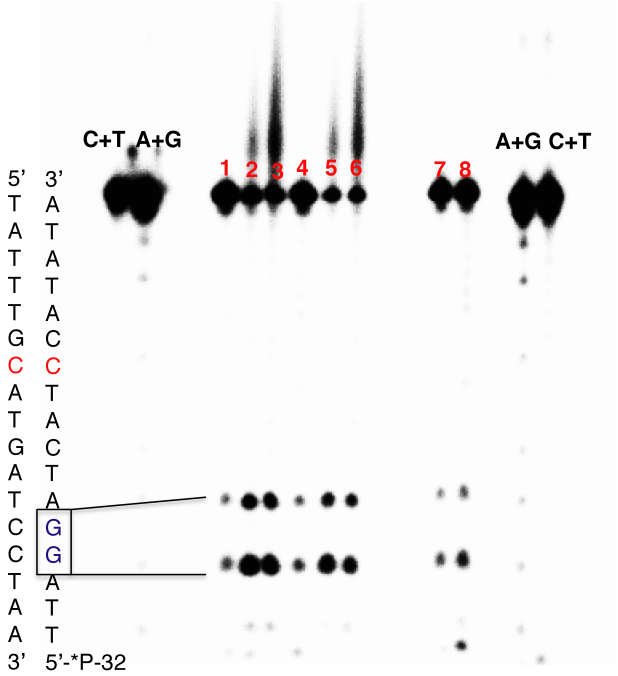

Figure 4.9 Dimethyl sulfate (DMS) footprinting of 5’-end radiolabeled duplex DNA containing a CC mismatch (denoted in red) and a d(GpG) site (denoted in blue, boxed). Samples were incubated with platinum and treated with 10% DMS, followed by piperidine cleavage. Samples were electrophoresed on a 20% denaturing PAGE gel. Lanes: (1) CC-mismatched DNA in the absence of platinum; (2) mismatched DNA with 1 μM conjugate; (3) mismatched DNA with 5 μM conjugate; (4) well-matched DNA in the absence of platinum; (5) well-matched DNA with 1 μM conjugate; (6) well-matched DNA with 5 μM conjugate; (7) mismatched DNA with 1 μM cisplatin; (8) well-matched DNA with 1 μM cisplatin; Maxam-Gilbert sequencing lanes (C+T; A+G) are located on the far left and far right of the gel. Bands of high electrophoretic mobility below the unmodified parent bands represent sites of guanine cleavage.

bromide). Metabolically active cells reduce MTT to formazan, which has a characteristic absorbance at 570 nm. Quantification of formazan by electronic absorption indicates the amount of viable cells in each sample.[31] The isogenically matched human colorectal carcinoma cell lines HCT116N (MMR-proficient) and HCT116O (MMR-deficient) as well as cisplatin-resistant A2780cis human ovarian cancer cells were plated in 96-well plates at 5.0 x 10^5 cells/well and treated with varying concentrations of $[Rh(chrysi)(phen)(DPE\text{-}Pt(NH_3)_2Cl)]^{3+}$. Cells were also treated with each parent subunit, $[Rh(chrysi)(phen)(DPE)]^{2+}$ and cisplatin, for 72h under humidified atmosphere. Percent viability is defined as the ratio of the amount of formazan in treated cells to that of untreated cells. The cytotoxic effects of the complexes in the HCT116N and HCT116O cell lines are shown in **Figure 4.10**.

As expected, the $[Rh(chrysi)(phen)(DPE)]^{2+}$ parent complex displays cell-selective cytotoxicity in the MMR-deficient HCT116O line, with an IC_{50} value of approximately 3.5 μM. Cisplatin exhibits no effect in either cell line, possibly due to being administered from saline solution, to provide an adequate control for the $[Rh(chrysi)(phen)(DPE\text{-}Pt(NH_3)_2Cl)]^{3+}$ complex, which is also prepared in aqueous NaCl (20 mM). The conjugate displays intermediary cytotoxic effects compared to its monomeric rhodium and platinum subunits: the cell-selectivity of the rhodium subunit is abolished, as both MMR-proficient and MMR-deficient cell lines are targeted equally. However, the conjugate exhibits enhanced potency compared to its platinum subunit ($IC_{50} \approx 10$ μM), signifying that conjugation to rhodium does play some role in enhancing the efficacy of the cisplatin parent complex, either through increased cellular uptake or DNA targeting. The potency of $[Rh(chrysi)(phen)(DPE\text{-}Pt(NH_3)_2Cl)]^{3+}$ is also

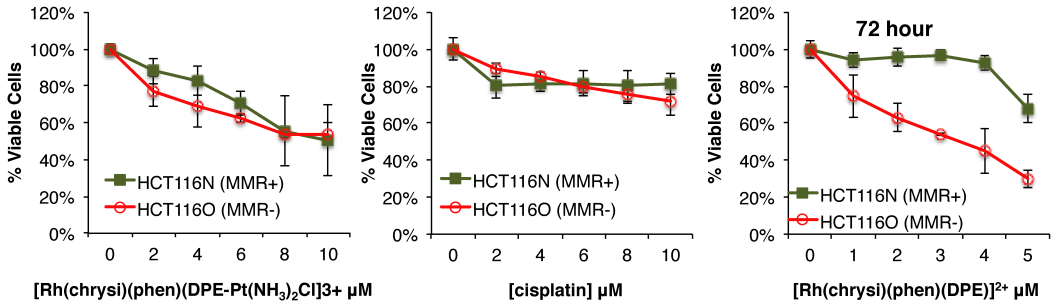

Figure 4.10 MTT cytotoxicity assay of HCT116N (MMR-proficient) and HCT116O (MMR-deficient) cells treated with $[Rh(chrysi)(phen)(DPE\text{-}Pt(NH_3)_2Cl)]^{3+}$ (left), cisplatin (center), and $[Rh(chrysi)(phen)(DPE)]^{2+}$. Cells were incubated with each complex at the concentrations indicated for 72h. After the incubation period, cells were treated with the MTT reagent for 4 h, and the resulting formazan crystals were solubilized with acidified SDS. Percent cell viability is defined as the percentage of formazan normalized to that of untreated cells. Standard errors were calculated from 5 replicates.

comparable to the previous-generation metalloinsertor-oxaliplatin conjugate, which has an IC_{50} value of 9 μM in the HCT116O cell line.[26]

The complexes were also examined in the cisplatin-resistant ovarian carcinoma A2780cis cell line (**Figure 4.11**). At 5 μM treatment, [Rh(chrysi)(phen)(DPE-$Pt(NH_3)_2Cl$)]$^{3+}$ imparts a 19% decrease in cell viability compared to cisplatin (and a 30% decrease in viability compared to untreated cells); however, the conjugate is less potent, albeit by a small margin, than [Rh(chrysi)(phen)(DPE)]$^{2+}$ or both rhodium and platinum subunits added separately.

4.3.3 Caspase and PARP Inhibition Assays

Characterization of a previous metalloinsertor-platinum conjugate revealed that the cytotoxic effects arose not from the necrotic cell death mechanism induced by monomeric metalloinsertors,[21] but rather through an apoptotic pathway more characteristic of *cis*-platinum complexes.[26,32,33] Here, we examined whether [Rh(chrysi)(phen)(DPE-$Pt(NH_3)_2Cl$)]$^{3+}$ also triggers apoptosis, which may account for its lack of cell-selectivity. HCT116N and HCT116O cells were treated with conjugate (5 μM) and poly-ADP ribose polymerase (PARP) inhibitor 3,4-dihydro-5[4-(1-piperindinyl)butoxy]-1(2*H*)-isoquinoline ("DPQ," 50 μM)[34] for 72h, and cell viability was assayed by MTT. Cells were treated similarly with DPQ (50 μM) and cisplatin (5 μM) as a control. The addition of PARP inhibitor DPQ protects cells from necrotic death, as PARP mediates this pathway through severe depletion of cellular ATP.[35] As can be seen in **Figure 4.12**, treatment of both cell lines with DPQ alone effects no change in viability. Similarly, DPQ has no effect on the viability of cells treated with [Rh(chrysi)(phen)(DPE-$Pt(NH_3)_2Cl$)]$^{3+}$. HCT116N cells exhibit 66 ± 2.0% cell viability

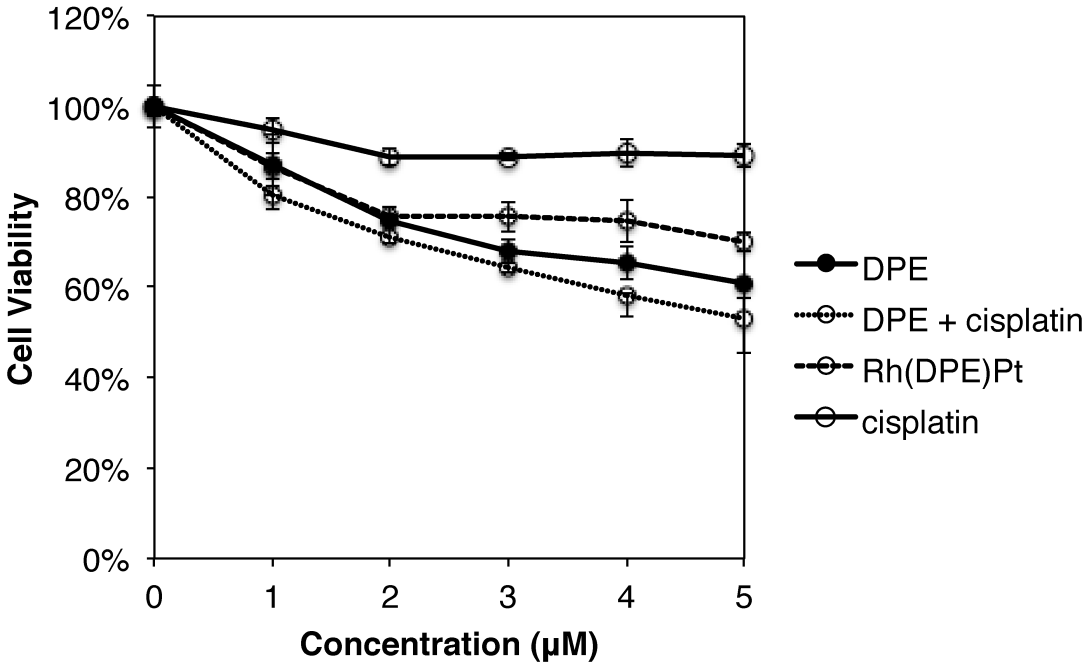

Figure 4.11 MTT cytotoxicity assay of cisplatin-resistant A2780cis cells treated with $[Rh(chrysi)(phen)(DPE)]^{2+}$ ("DPE," solid line, closed circles), cisplatin (solid line, open circles), a combination of $[Rh(chrysi)(phen)(DPE)]^{2+}$ and cisplatin ("DPE + cisplatin," dotted line, open circles), and $[Rh(chrysi)(phen)(DPE\text{-}Pt(NH_3)_2Cl)]^{3+}$ ("Rh(DPE)Pt," dashed line, open circles). Cells were incubated with each complex at the concentrations indicated for 72h. After the incubation period, cells were treated with the MTT reagent for 4 h, and the resulting formazan crystals were solubilized with acidified SDS. Percent cell viability is defined as the percentage of formazan normalized to that of untreated cells. Standard errors were calculated from 5 replicates.

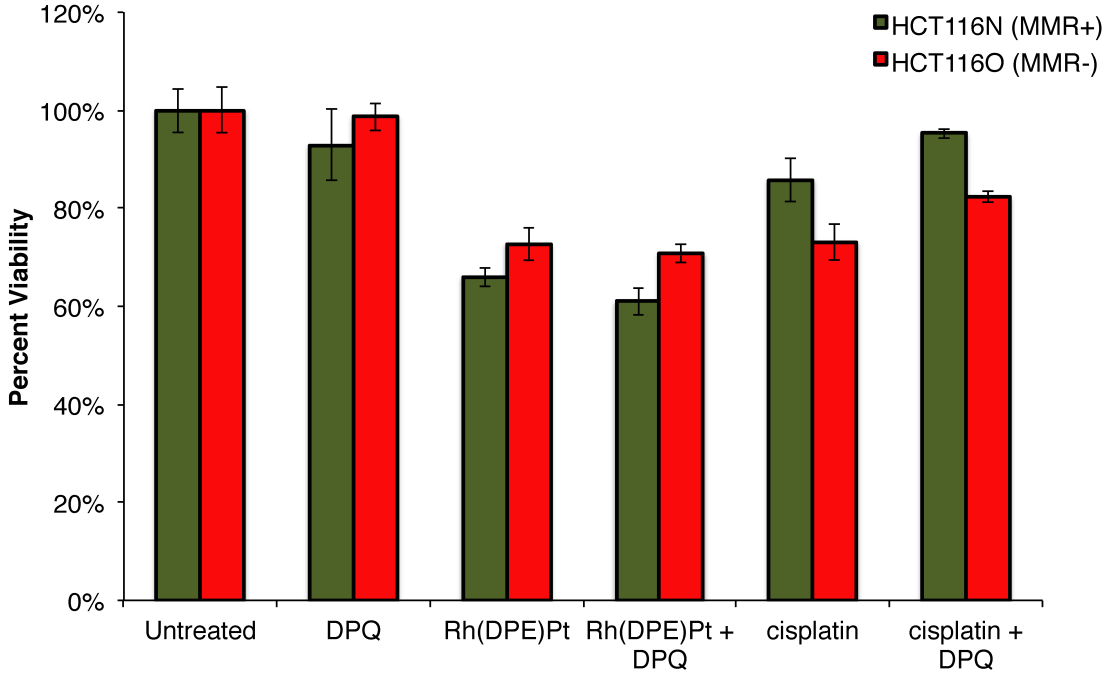

Figure 4.12 Cell viability in HCT116N (green, MMR-proficient) and HCT116O (red, MMR-deficient) cells after 72h treatment with PARP inhibitor DPQ. Viability is normalized to untreated controls. Treatment with DPQ (50 μM) alone has no effect on cell viability. Likewise, DPQ does not increase the viability of cells treated with [Rh(chrysi)(phen)(DPE-Pt(NH_3)$_2$Cl]$^{3+}$ ("Rh(DPE)Pt," 5 μM). A modest increase in viability is observed when cells are exposed to DPQ in combination with cisplatin (5 μM).

in the presence of conjugate alone, and 61 ± 2.8% viability with metal complex administered in combination with PARP inhibitor. For HCT116O cells, viability is 73 ± 3.4% and 71 ± 2.0% in the presence of the conjugate alone and the combination treatment, respectively. These results indicate that the cytotoxic effects of $[Rh(chrysi)(phen)(DPE\text{-}Pt(NH_3)_2Cl)]^{3+}$ in HCT116 cells are independent of the PARP pathway and therefore do not proceed via necrosis.

Curiously, co-treatment of cells with cisplatin (5 μM) an DPQ (50 μM) results in a statistically significant increase ($p < 0.0001$ by unpaired two-tailed t test) in cell viability compared to treatment with cisplatin alone: the percentage of viable HCT116N cells increases from 86 ± 4.3% to 95 ± 1.0% upon the addition of PARP inhibitor, and the fraction of viable HCT116O cells increases from 73 ± 3.6% to 82 ± 1.1%. While these are modest changes overall, these results suggest that cisplatin induces necrosis in these cell lines to some degree.

The experiment was also performed in the presence of a pan-caspase inhibitor, Z-VAD-FMK. By irreversibly binding to the active site of caspases, Z-VAD-FMK inhibits apoptosis.[36] Previously, it has been shown that appendage of a platinum moiety to a metalloinsertor triggers caspase-dependent cell death, signifying apoptosis rather than necrosis.[26] Here, treatment of HCT116N and HCT116O cells with $[Rh(chrysi)(phen)(DPE\text{-}Pt(NH_3)_2Cl)]^{3+}$ in combination with caspase inhibitor results in a similar outcome. Cells were treated with $[Rh(chrysi)(phen)(DPE\text{-}Pt(NH_3)_2Cl)]^{3+}$ (5 μM) or cisplatin (5 μM) in combination with Z-VAD-FMK (35 μM) for 72h, and cell viability was determined by MTT cytotoxicity assay (**Figure 4.13**).

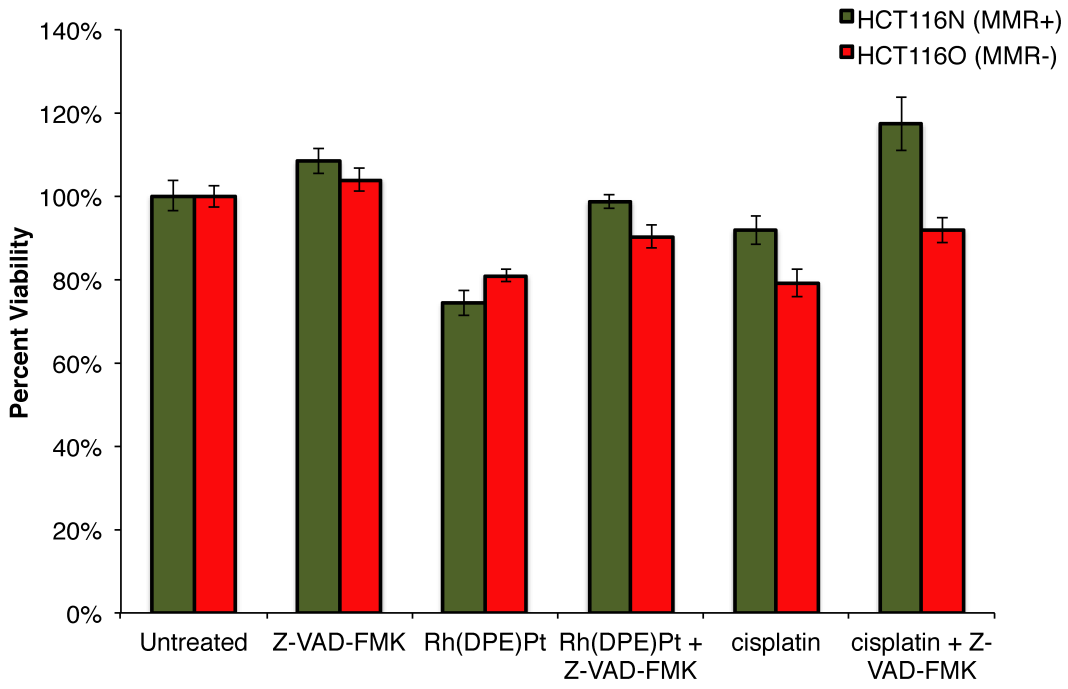

Figure 4.13 Cell viability in HCT116N (green, MMR-proficient) and HCT116O (red, MMR-deficient) cells after 72h treatment with caspase inhibitor Z-VAD-FMK. Viability is normalized to untreated controls. Treatment with Z-VAD-FMK (35 μM) alone has no effect on cell viability. When administered in combination with [Rh(chrysi)(phen)(DPE-$Pt(NH_3)_2Cl]^{3+}$ ("Rh(DPE)Pt," 5 μM), a statistically significant increase in viability is observed in both cell lines. A similar result is observed when capase inhibitor is added in combination with cisplatin (5 μM). These results signify caspase-dependent apoptosis ($p < 0.0001$ by unpaired two-tailed t-test).

A clear increase in cell viability upon addition of the caspase inhibitor is observed for both cell lines treated with conjugate. In fact, caspase inhibition almost completely abolishes the cytotoxic effects of the conjugate: the percentage of viable HCT116N cells increases from 74 ± 3.0% with $[Rh(chrysi)(phen)(DPE\text{-}Pt(NH_3)_2Cl)]^{3+}$ alone to 99 ± 1.6% upon addition of Z-VAD-FMK, and the percentage of viable HCT116O cells is similarly enhanced from 81 ± 1.5% to 90 ± 2.7%. For both cell lines, these differences were determined to be statistically significant by unpaired two-tailed *t*-test ($p < 0.0001$). These results, in combination with the results of the MTT assay in combination with PARP inhibitor, signify that the cytotoxicity of $[Rh(chrysi)(phen)(DPE\text{-}Pt(NH_3)_2Cl)]^{3+}$ is caspase-dependent and PARP-independent. $[Rh(chrysi)(phen)(DPE\text{-}Pt(NH_3)_2Cl)]^{3+}$ induces an apoptotic mode of cell death in both HCT116N and HCT116O cell lines.

The cisplatin-treated cells display similar results upon addition of Z-VAD-FMK: cell viability increases 25 ± 2.9% and 13 ± 0.3% for HCT116N and HCT116O cells, respectively, compared to treatment with cisplatin alone ($p < 0.0001$ by unpaired two-tailed *t* test). Exposure of cisplatin-treated cells to caspase inhibitor results in a markedly more dramatic increase in cell viability compared to treatment with PARP inhibitor, suggesting that while some cells may be undergoing necrotic cell death, the apoptotic pathway is likely the major mechanism of cisplatin cytotoxicity.

4.4 Discussion

4.4.1 Synthesis of $[Rh(chrysi)(phen)(DPE\text{-}Pt(NH_3)_2Cl)]^{3+}$

We have synthesized a new bimetallic Rh-Pt metalloinsertor derived from a recently characterized family of complexes bearing axial Rh—O bonds.[24] Metalloinsertors containing these ligands, which coordinate through a five-membered

pyridylethanol ring, have been shown to exhibit enhanced potency and cell-selectivity in MMR-deficient cells.[22,24] Furthermore, these complexes can accommodate a wide variety of functional groups incorporated into the *N,O*-coorindating ligand without sacrificing DNA binding ability or biological activity, making this class of complexes an attractive scaffold for the development of next-generation bifunctional metalloinsertor conjugates.

The metalloinsertor parent complex, $[Rh(chrysi)(phen)(DPE)]^{2+}$ (**Figure 4.1**), contains a non-coordinating pyridine functionality within the pyridyl-ethanol ligand scaffold. This extraneous pyridine serves as the site of coordination for cisplatin. Simple reflux of commercially available cisplatin with the rhodium parent complex under acidic conditions displaces one of the labile chloride ligands on the platinum center, affording $[Rh(chrysi)(phen)(DPE\text{-}Pt(NH_3)_2Cl)]^{3+}$ (**Figure 4.1**) in a single step in reasonable yield (**Scheme 4.1**). This conjugate, then, contains a platinum center with only a single labilization site at the remaining chloride, and is therefore expected to form "monofunctional" platinum adducts – that is, the platinum will only coordinate a single nucleobase on the DNA, rather than binding two nearby residues and forming the classical 1,2- or 1,3-intrastrand crosslinks characteristic of the cisplatin parent complex.

Monofunctional platinum anticancer complexes, particularly those with the general structure *cis*-$[Pt(NH_3)_2(L)Cl]^+$ (where L is an N-heterocycle), have been heavily investigated by Lippard and others.[37-40] Long considered to be clinically irrelevant due to the inactivity of the first studied monofunctional compounds, $[Pt(dien)Cl]^+$ (dien = diethylenetriamine) and $[Pt(NH_3)_3Cl]^+$,[41-43] interest in this class of complexes has been renewed in recent years with the development of more active analogues, such as pyriplatin (*cis*-$[Pt(NH_3)_2(pyridine)Cl]^{2+}$)[44] and the highly potent phenanthriplatin (*cis*-

[$Pt(NH_3)_2$(phenanthridine)Cl](NO_3)), which is being investigated as a new chemotherapeutic agent.[45,46] These complexes have been shown to form monofunctional adducts with single bases on DNA, usually at the *N*7 position of guanine.[37,44] These crosslinks distort the DNA in a manner that is structurally distinct from that of cisplatin and other bifunctional *cis*-platinum (II) complexes, resulting in considerably less bending and unwinding of the DNA.[47-50] These complexes thus exert their anticancer activity via different biological mechanisms, providing orthogonality in the treatment of cisplatin-resistant cancers.[47] In addition to the distinctive DNA binding exhibited by *cis*-$[Pt(NH_3)_2(L)Cl]^+$ complexes, the presence of the bulky N-heterocycle protects the metal center from deactivating protein thiols as well as recognition by nucleotide excision repair proteins, which repair Pt-DNA adducts and lead to resistance.[37,44,51] As a result, monofunctional, cationic platinum (II) complexes are a growing class of platinum-based drugs that can be effective against cisplatin-resistant cancers.

The synthesis and characterization of $[Rh(chrysi)(phen)(DPE\text{-}Pt(NH_3)_2Cl)]^{3+}$ represents the first example of a monofunctional platinum complex conjugated to a rhodium metalloinsertor, as well as the first example of a bifunctional conjugate developed from the Rh—O metalloinsertor family. The DNA binding behavior of the complex has been characterized *in vitro*, and the cytotoxic activity was explored in three human cancer cell lines.

4.4.2 DNA Binding Behavior

The $[Rh(chrysi)(phen)(DPE\text{-}Pt(NH_3)_2Cl)]^{3+}$ was designed as previous iterations of Rh-Pt metalloinsertor conjugates, comprising a rhodium (III) subunit coordinated to a 5,6-chrysenequinone diimine ligand for base pair mismatch recognition and a thermally

activated platinum subunit for covalent DNA binding. The complex was analyzed for both mismatch binding and platinum crosslinking on hairpin and duplex radiolabeled DNA containing a CC mismatch. The conjugate is capable of simultaneous metalloinsertion at a mismatch and platinum adduct formation with hairpin DNA (**Figure 4.3**). Additionally, platinum binding was explored with mismatched and well-matched duplex DNA, and it was revealed that the complex preferentially binds mismatched DNA over well-matched sequences.

The preferential platination of mismatched DNA over well-matched *in vitro* likely results from the ability of the complex to target mismatched sites in DNA by metalloinsertion. This behavior has been shown previously in our laboratory with a metalloinsertor-cisplatin conjugate.[25] Here, the rhodium and platinum subunits were separated by a six-carbon alkyl linker region, and metalloinsertion at a mismatch successfully directed platinum binding preferentially toward mismatched DNA over a well-matched duplex. However, this preferential binding was highly dependent on the presence and location of a d(GpG) site (the preferred binding site of cisplatin); if there was no d(GpG) site, or if it was inaccessible to the platinum center due to limitations in the length and flexibility of the alkyl tether (i.e., situated too closely to the site of the mismatch), then minimal platination occurred. Likewise, there was no preference for mismatched DNA in these scenarios. Selective DNA platination, then, is highly sequence-dependent for this complex.

The structural limitations of the first-generation metalloinsertor-platinum conjugate do not appear to be present for $[Rh(chrysi)(phen)(DPE\text{-}Pt(NH_3)_2Cl)]^{3+}$, despite the fact that the platinum subunit is considerably more constricted in its coordination to

the DPE ligand. The complex has been shown to platinate mismatched (and, to a lesser extent, well-matched) DNA in both hairpin and duplex sequences (See **Section 4.3.1.1** and **4.3.1.2** for sequences), including variation in the sequence context surrounding the site of the CC mismatch. Furthermore, in the case of the duplex DNA sequence, the d(GpG) site is located six and seven base pairs away from the mismatch – an unreachable distance for simultaneous metalloinsertion and platination by a complex with virtually no separation between the subunits.

We considered the possibility that the simultaneous mismatch binding and crosslinking could be the result of two or more equivalents of the complex binding to different sites on the DNA – one equivalent at the mismatch, which in turn stabilizes the duplex for coordination of a second equivalent at the distal d(GpG) site. However, DNA sequencing of the guanine residues by DMS footprinting revealed that $[Rh(chrysi)(phen)(DPE\text{-}Pt(NH_3)_2Cl)]^{3+}$ does not form covalent adducts with either guanine on the radiolabeled strand. In fact, the binding of the conjugate results in an increase in the efficiency of guanine methylation by DMS (rather than the decrease that would be expected for platinum bound at that site), implying that the site of platination potentially distorts and/or unwinds the DNA helix in a manner that leaves the guanines more accessible to methylation.

It is currently unclear what the preferred site of coordination is for the conjugate. Preliminary DNA sequencing studies reveal no evidence of adenine binding (data not shown). The *N*3 position of cytosine is nucleophilic enough to coordinate platinum – early models of monofunctional platinum complexes contained *N*3-cytosine as the N-heterocyclic ligand[48] – however, it is surprising that the considerably more nucleophilic

guanine and adenine *N*7 positions are not favored binding sites, even in the case of well-matched DNA. Coordination at cytosine *N*3 has been observed in a DNA oligomer, but is uncommon and typically occurs as part of a bifunctional coordination with an adjacent guanine.[49] This unusual DNA binding behavior of $[Rh(chrysi)(phen)(DPE\text{-}Pt(NH_3)_2Cl)]^{3+}$ possibly contributes to the mismatch-selectivity of the complex *in vitro*: because coordination with the most nucleophilic sites on DNA is disfavored, coordination of the platinum center is thermodynamically directed by metalloinsertion at mismatched sites from the minor groove.

In previous generations of metalloinsertor-platinum conjugates, the rhodium and platinum subunits functioned essentially as separate entities, even in instances where platination was directed towards mismatched DNA by the rhodium subunit. This was due to the construction of the conjugates either as metastable, hydrolysable subunits or two permanently linked functionalities separated by a long, flexible alkyl chain.[25,26] In the case of $[Rh(chrysi)(phen)(DPE\text{-}Pt(NH_3)_2Cl)]^{3+}$, however, both metal centers directly coordinate the relatively small DPE ligand, placing them in close proximity to one another and offering little flexibility for the subunits to function independently of one another. Therefore, it is possible that the nature of the observed platinum coordination is informed by the unusual DNA binding behavior already exhibited by the $[Rh(chrysi)(phen)(DPE)]^{2+}$ parent complex. To explain the accommodation of the bulky, "dangling" pyridine in the minor groove, as well as the mismatch binding ability of the Λ-enantiomer to B-form DNA, an alternate mode of metalloinsertion has been proposed, involving a side-on insertion of the buckled chrysi ligand such that only two benzene rings are incorporated into the nucleobase stack.[24] This binding mode may situate the

platinum center in a position favorable for crosslinking; however, it does not explain how the complex binds to well-matched DNA. Additional studies are necessary to further understand the nature of the DNA binding behavior of this bimetallic conjugate.

4.4.3 Characterization in Cell Tissue Culture

Encouraged by the mismatch specificity exhibited by [Rh(chrysi)(phen)(DPE-$Pt(NH_3)_2Cl$)]$^{3+}$ *in vitro*, we sought to examine whether this translated to cell-selective cytotoxicity in cancer cells deficient in mismatch repair. The cytotoxic effects of the conjugate were explored in the isogenic human colorectal carcinoma cell lines HCT116N (MMR-proficient) and HCT116O (MMR-deficient) as well as the cisplatin-resistant human ovarian cancer line A2780cis. While the conjugate does not display the potency or cell-selective targeting of HCT116O cells exhibited by its [Rh(chrysi)(phen)(DPE)]$^{2+}$ parent complex, it outperforms its other parent complex, the FDA-approved chemotherapeutic cisplatin, in all three cell lines. The lack of selective targeting of MMR-deficient cells is attributed to the complex triggering an apoptotic, rather than necrotic, mode of cell death as determined by cytotoxicity assays performed with caspase and PARP inhibitors. As has been seen previously, the appendage of a platinum (II) functionality circumvents the biological response to genomic mismatch recognition by metalloinsertors, resulting in a toxic but nonspecific apoptotic response.[26]

Although the cell-specific biological activity of the [Rh(chrysi)(phen)(DPE)]$^{2+}$ metalloinsertor could not be transferred to a cytotoxic platinum subunit, [Rh(chrysi)(phen)(DPE-$Pt(NH_3)_2Cl$)]$^{3+}$ is quite efficacious for a monofunctional *cis*-platinum (II) compound. Early examples of monofunctional platinum complexes, such as [Pt(dien)Cl]$^{+}$ and [$Pt(NH_3)_3Cl$]$^{+}$, display no cytotoxicity *in cellulo*.[41-43] Pyriplatin, the

exploratory lead compound for monofunctional platinum complexes and a close structural analogue of the platinum subunit of $[Rh(chrysi)(phen)(DPE\text{-}Pt(NH_3)_2Cl)]^{3+}$, also exhibits limited potency, with reported IC_{50} values surpassing 200 μM for HCT116 cells as well as a spectrum of various cancer cell lines.[52] Indeed, aside from phenanthriplatin, there are few examples of monofunctional platinum (II) complexes that surpass cisplatin in potency, despite the evaluation of many derivations of these complexes in a variety of cancer cell lines.[45] It is presently unclear precisely how the rhodium subunit enhances the efficacy of the monofunctional platinum center in this conjugate; it is possible that properties such as increased lipophilicity and charge afforded by attachment of the metalloinsertor enhances cellular uptake, as was seen for the previously reported metalloinsertor-oxaliplatin complex.[26] Perhaps the bulky rhodium center shields the platinum moiety from deactivating proteins or creates a bulky lesion that blocks DNA synthesis, as is observed with phenanthriplatin.[51] Future studies may further probe the underlying biological mechanisms of this unusual complex.

4.5 Conclusions

Here we report the synthesis, *in vitro* characterization, and biological evaluation of a bimetallic Rh(III)-Pt(II) metalloinsertor conjugate that incorporates both the unusual ligand coordination of a recently characterized family of metalloinsertors as well as a monofunctional *cis*-$[Pt(NH_3)_2(N\text{-heterocycle})Cl]^+$ subunit. While not cell-selective, the conjugate displays increased potency compared to FDA-approved cisplatin in all cell lines studied. Moreover, the complex exhibits enhanced platination of mismatched over well-matched DNA *in vitro*, which may arise from uncharacteristic crosslinking of an alternative base preferentially over guanine by platinum in addition to mismatch

recognition by the rhodium subunit. The results herein confirm that rhodium metalloinsertors containing axial Rh—O bonds can be developed as scaffolds for conjugation, resulting in selective targeting of their cargo towards mismatched DNA. The ease with which these complexes can be functionalized enables the development of future conjugates incorporating alternative functionalities, such as cell-penetrating peptides or antibodies. This work also provides the foundation for exploration into non-classical platinum complexes that deviate from traditional structure-activity rules as potential mismatch-targeting agents.

3.6 References

1 Wang, D.; Lippard, S. J. *Nature Rev. Drug Discov.* **2005**, *4*, 307-320.

2 Jamieson, E. R., Lippard, S. J. *Chem. Rev.* **1999**, *99*, 2467-2498.

3 Decatris, M. P., Sundar, S., O'Byrne, K. J. *Cancer Treat. Rev.* **2004**, *30*, 53–81.

4 Fink, D.; Aebi, S.; Howell, S. B. *Clin. Cancer Res.* **1998**, *4*, 1-6.

5 Aebi, S.; Fink, D.; Gordon, R.; Kim, H. K.; Zheng, H.; Fink, J. L.; Howell, S. B. *Clin. Cancer Res.* **1997**, *3*, 1763-1767.

6 Dulhunty, A. F. *J. Physiol.* **1978**, *276*, 67-82.

7 Kehe, K.; Szinicz, L. *Toxicology* **2005**, *214*, 198-209.

8 Reedijk, J. *Chem. Rev.* **1999**, *99*, 2499-2510.

9 Jackson, B. A.; Barton, J. K. *J. Am. Chem. Soc.* **1997**, *119*, 12986–12987.

10 Loeb, L. A. *Cancer Res.* **2001**, *61*, 3230-3239.

11 Bhattacharya, N. P.; Skandalis, A.; Ganesh, A.; Groden, J.; Meuth, M. *Proc. Natl. Acad. Sci. U.S.A.* **1994**, *91*, 6319-6323.

12 Carethers, J. M.; Hawn, M. T.; Chauhan, D. P.; Luce, M. C.; Marra, G.; Koi, M.; Boland, C. R. *J. Clin. Invest.* **1996**, *98*, 199-206.

13 Jackson, B. A.; Barton, J. K. *Biochemistry* **2000**, *39*, 6176–6182.

14 Jackson, B. A.; Alekseyev, V. Y.; Barton, J. K. *Biochemistry* **1999**, *38*, 4655–4662.

15 Pierre, V. C.; Kaiser, J. T.; Barton, J. K. *Proc. Natl. Acad. Sci. U.S.A.* **2007**, *104*, 429.

16 Cordier, C.; Pierre, V. C.; Barton, J. K. *J. Am. Chem. Soc.* **2007**, *129*, 12287–12295.

17 Zeglis, B. M.; Pierre, V. C.; Kaiser, J. T.; Barton, J. K. *Biochemistry* **2009**, *48*, 4247.

18 Song, H.; Kaiser, J. T.; Barton, J. K. *Nature Chem.* **2012**, *4*, 615–620.

19 Hart, J. R.; Glebov, O.; Ernst, R. J.; Kirsch, I. R.; Barton, J. K. *Proc. Natl. Acad. Sci. U.S.A.* **2006**, *103*, 15359–15363.

20 Ernst, R. J.; Song, H.; Barton, J. K. *J. Am. Chem. Soc.* **2009**, *131*, 2359–2366.

21 Ernst, R. J.; Komor, A. C.; Barton, J. K. *Biochemistry* **2011**, *50*, 10919–10928.

22 Komor, A. C.; Schneider, C. J.; Weidmann, A. G.; Barton, J. K. *J. Am. Chem. Soc.* **2012**, *134*, 19223–19233.

23 Weidmann, A. G.; Komor, A. C.; Barton, J. K. *Philos. Trans. R. Soc. A.* **2013**, *371*, 20120117.

24 Komor, A. C.; Barton, J. K. *J. Am. Chem. Soc.* **2014**, *136*, 14160-14172.

25 Petitjean, A.; Barton, J. K. *J. Am. Chem. Soc.* **2004**, *126*, 14728-14729.

26 Weidmann, A. G.; Barton, J. K. *Inorg. Chem.* **2014**, *53*, 7812-7814.

27 Ernst, R. J. *Unpublished results*

28 Basu, A.; Bhaduri, S.; Sapre, N. Y.; Jones, P. G. *J. Chem. Soc., Chem. Commun.* **1987**, *22*, 1724−1725.

29 Muerner, H.; Jackson, B. A.; Barton, J. K. *Inorg. Chem.* **1998**, *37*, 3007-3012.

30 Brabec, V.; Leng, M. *Proc. Natl. Acad. Sci. U.S.A.* **1993**, *90*, 5345-5349.

31 Mosmann, T. *J. Immunol. Methods* **1983**, *65*, 55-63.

32 Siddik, Z. H. *Oncogene* **2003**, *22*, 7265.

33 Arango, D.; Wilson, A. J.; Shi, Q.; Corner, G. A.; Arañes, M. J.; Nicholas, C.; Lesser, M.; Mariadason, J. M.; Augenlicht, L. H. *Br. J. Cancer* **2004**, *91*, 1931.

34 Costantino, G., Macchiarulo, A., Camaioni, E., and Pellicciari, R. *J. Med. Chem.* **2001**, *44*, 3786-3794.

35 Ha, H.C., Snyder, S. H. *Proc. Natl. Acad. Sci. U.S.A.* **1999**, *96*, 13978-13982.

36 Vandenabeele, P., Vanden Berghe, T., and Festjens, N. *Sci. STKE*, **2006**, *358*, pe44.

37 Johnstone, T. C.; Wilson, J. J.; Lippard, S. J. *Inorg. Chem.* **2013**, *52*, 12234-12249.

38 Hollis, L. S.; Amundsen, A. R.; Stern, E. W. *J. Med. Chem.* **1989**, *32*, 128-136.

39 Baird, C. L.; Griffitts, A. E.; Baffic, S.; Bryant, P.; Wolf, B.; Lutton, J.; Berardini, M.; Arvanitis, G. M. *Inorg. Chim. Acta* **1997**, *256*, 253-262.

40 Sundquist, W. I.; Bancroft, D. P.; Lippard, S. J. *J. Am. Chem. Soc.* **1990**, *112*, 1590-1596.

41 Macquet, J. P.; Butour, J. L. *J. Natl. Cancer Inst.* **1983**, *70*, 899-905.

42 Brabec, V.; Reedijk, J.; Leng, M. *Biochemistry* **1992**, *31*, 12397-12402.

43 Bursova, V.; Kasparkov, J.; Hofr, C.; Brabec, V. *Biophys. J.* **2005**, *88*, 1207-1214.

44 Lovejoy, K. S.; Todd, R. C.; Zhang, S.; McCormick, M. S.; D'Aquino, J. A.; Reardon, J. T.; Sancar, A.; Giacomini, K. M.; Lippard, S. J.

45 Park, G. Y.; Wilson, J. J.; Song, Y.; Lippard, S. J. *Proc. Natl. Acad. Sci. U.S.A.* **2012**, *109*, 11987-11992.

46 Johnstone, T. J.; Park, G. Y.; Lippard, S. J. *Anticancer Res.* **2014**, *34*, 471-476.

47 Lempers, E. L. M.; Bloemink, M. J.; Brouwer, J.; Kidani, Y.; Reedijk, J. *J. Inorg. Biochem.* **1990**, *40*, 23-25.

48 Bellon, S. F.; Lippard, S. J. *Biophys. Chem.* **1990**, *35*, 179-188.

49 Chottard, J. C.; Ledner, J. A.; Bauer, W. A.; Ushay, H. M.; Caravana, C.; Lippard, S. J. *J. Am. Chem. Soc.* **1980**, *102*, 2487-2488.

50 Keck, M. V.; Lippard, S. J. *J. Am. Chem. Soc.* **1992**, *114*, 3386-3390.

51 Wang, D.; Zhu, G.; Huang, X.; Lippard, S. J. *Proc. Natl. Acad. Sci. U.S.A.* **2010**, *107*, 9584-9589.

52 Lovejoy, K. S.; Serova, M.; Bieche, I.; Emami, S.; D'Incalci, M.; Broggini, M.; Erba, E.; Gespach, C.; Cvitkovic, E.; Faivre, S.; Raymond, E.; Lippard, S. J. *Mol. Cancer Ther.* **2011**, *10*, 1709-1719.